Influence of the distribution of the inherent ordering temperature on the ordering in layered magnets

Moreno Marcellini, Martin Pärnaste, and Björgvin Hjörvarsson*
Department of Physics, Uppsala University, Box 530, 75121 Uppsala, Sweden

Maximilian Wolff
Institut Laue-Langevin, F-38042 Grenoble Cedex 9, France

(Received 28 February 2008; revised manuscript received 12 February 2009; published 22 April 2009)

We study the influence of gradients in the inherent ordering temperature of coupled layered magnets on the overall magnetic ordering. The gradients were accomplished by growing Fe(001) layers with thicknesses ranging from two to three monolayers, all separated by seven monolayers of V(001). Two types of *gradient* superstructures were grown: one with the highest and one with the lowest inherent ordering temperature in the center of the samples. The superstructure with the thinnest outermost Fe layers exhibits lower ordering temperature, demonstrating the importance of the sequence of the layers. Both these structures order at temperatures significantly lower than a superlattice with a constant thickness of the Fe layers (three monolayers). The results highlight the intricate collective aspects of the magnetic ordering in layered magnets, which are not captured by current models in magnetism research.

DOI: 10.1103/PhysRevB.79.144426 PACS number(s): 75.40.Cx, 75.50.Bb, 75.70.−i

I. INTRODUCTION

The magnetic ordering in multilayered magnetic materials depends strongly on both the interlayer (J') (Refs. 1–4) as well as the intralayer (J) coupling.[5,6] Multilayered magnetic structures offer therefore a unique possibility to explore the influence of these important parameters, separating their contributions, and thereby providing important tests of theoretical concepts and models. The ordering of the magnetic layers can be ferromagnetic (FM) or antiferromagnetic (AFM) in a multilayer because the sign and the strength of J' depend on the thickness of the nonmagnetic spacer layer.[7,8] Also, the tuning of J' offers the possibility to adjust the ordering temperature (T_c), as discussed in Refs. 2, 3, and 9–12. The exploration of the influence of coupling between two magnetic layers with different ordering temperatures has previously been studied by Baberschke and co-workers[11,13,14] by using the x-ray magnetic dircular dichroism (XMCD) technique. By using two different elements combined with the element specificity of XMCD, they demonstrated unexpectedly large shifts in the ordering temperatures of the layers. The temperature dependence of the interlayer exchange coupling and its effect on the magnetic excitations have also been studied,[4,15] highlighting the intricate relation between the spin-wave excitations and the effective interlayer coupling.

The inherent ordering temperature of a single layer is determined by the thickness of the magnetic layer,

$$T_c(l) = T_c(\infty)[1 - bl^{-\lambda}], \tag{1}$$

where $T_c(\infty)$ denotes the ordering temperature of the bulk material, b is a constant, l is the thickness of the layer, and λ is the shift exponent.[16–18] It is therefore possible to eventually tailor the distribution of the inherent ordering temperature ($T_{c,i}$) of each layer in a multilayer by the choice of the thickness of the (ith) layer. The influence of the interlayer coupling can be chosen by the selected thickness of the nonmagnetic spacer layers. This idea is illustrated in Fig. 1, using Fe(001) and V(001) layers as an example. The influence of the thickness of the Fe and V layers on T_c is well known. T_c increases linearly with ≈200 K per monolayer (ML) of Fe (Ref. 6) while the change in T_c with the V thickness is much weaker and nonlinear[19] in the thickness range chosen for the present experiments. Thus, this material combination appears to be suitable in testing the influence of a distribution of $T_{c,i}$ on the overall ordering in coupled magnetic multilayers.

In the actual design, Fig. 1(b), the thickness of the thinnest Fe layer is two monolayers. The increase in the Fe thickness is equivalent to 0.05 monolayers/layer, reaching three monolayers of Fe in the 21st layer. The *inherent* ordering

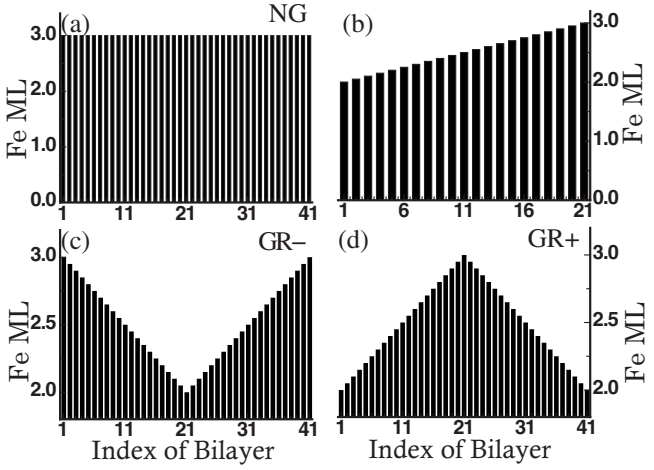

FIG. 1. The thickness profiles of the magnetic layers. The inherent ordering temperature of each Fe layer is proportional to its thickness. (a) illustrates a regular superlattice structure with constant thickness of all the layers while (b) resembles the building block used for obtaining a distribution in T_c. (c) illustrates the structure with the lowest inherent T_c in the center of the sample while (d) has the highest inherent ordering temperature in the center.

temperature of the layers is therefore changing from the ordering temperature of two monolayers to that of three monolayers of Fe. In the absence of coupling, the difference in the ordering temperature of the layers corresponds therefore to about 200 K.

It is possible to form two types of mirror symmetric profiles by using this design as a building block, as illustrated in Figs. 1(c) and 1(d). The profile with decreasing $T_{c,i}$ with increasing distance from the surface [see Fig. 1(c)] is denoted GR− (negative gradient) while the profile with increasing $T_{c,i}$ is denoted GR+ (positive gradient) [see Fig. 1(d)]. If the sign of the gradient in the inherent ordering temperature of the layers does not influence the overall ordering, identical results should be obtained for both these structures. However, if the sign is relevant, the overall ordering temperature will not be the same. Thus, these two types of arrangements appear to be suitable to study the influence of the variation in the inherent ordering temperature, as well as the sequence, on the magnetic ordering. We used different techniques to access the magnetic ordering at all the relevant length scales, namely, the overall layer resolved as well as the near-surface magnetization. A superconducting quantum interference device (SQUID) was used to determine the total moment of the samples, as well as the changes in the magnetization with temperature. Neutron reflectivity was used to obtain the layer-by-layer changes in the magnetization and we used the magneto-optical Kerr effect (MOKE) to determine the temperature dependence of the near-surface magnetization. This approach allowed us to study the influence on the magnetic ordering of the boundaries as well as of the distribution of the inherent ordering temperature of the layers.

II. SAMPLE DESCRIPTION

In the present experiment we used Fe(001) and V(001) layers as building blocks. Fe/V superlattices exhibit Frank-van der Merwe growth mode resulting in high quality superlattices which have been used for exploring magnetic[1,3,6,20] and structural phase transitions[21,22] as well as transport properties of layered magnets.[23,24]

The samples were grown in a DCA four source sputtering chamber on MgO (001) $20\times20\times1$ mm^3 substrates from Crystal GmbH. The thickness of each layer was determined by timing the opening and the closing of the shutters. The first V layer was deposited on the MgO substrate and each superlattice was terminated by an extra V layer. In order to protect the samples from oxidation, a capping layer of Pd ≈50 Å was finally grown on the outermost V layer. The number of repetitions of the Fe/V bilayers was 41 and the thickness of the V layers was fixed at 7 ML.[25] The interlayer coupling J' can thereby be regarded as having fixed magnitude and sign. The samples are FM ordered, and J' is much smaller than J.[19] One of the samples was a regular superlattice (that is with fixed Fe thickness) based on the bilayer Fe_3/V_7 (the subscripts indicate the number of ML for each metal), hereafter called no gradient (NG), see Fig. 1(a). The other two samples were made using the building block illustrated in Fig. 1(b). The GR+ sample has 2 ML of Fe as the topmost and bottom-most magnetic layers, see Fig. 1(d), and the sample GR− has 3 ML of Fe as the topmost and bottom-most magnetic layers, see Fig. 1(c).

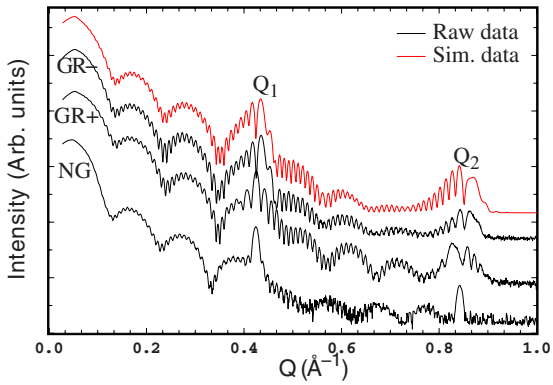

FIG. 2. (Color online) X-ray reflectivities obtained from the samples. The topmost curve is a representative fit for one of the samples (GR−, red). The superlattices peaks are well displayed at Q_1 and Q_2. The intensities are shifted for clarity.

III. STRUCTURAL CHARACTERIZATION

A structural characterization of the samples was carried out by x-ray reflectivity and diffraction in a Philips PW3020, equipped with a graphite monochromator. As seen in Fig. 2, the reflectivity data show features generally present in multilayer structures. The peaks denoted by Q_1 and Q_2 represent the superlattice peaks with positions determined by:[26]

$$\Lambda(Q_m^2 - Q_c^2)^{1/2} = 2\pi m, \tag{2}$$

where Λ is the thickness of the bilayer, Q_m is the scattering vector at the reflection m, and Q_c is the critical scattering vector.[27] The peak at Q_1 corresponds to the Fourier component of the bilayer repetition whereas the peak at Q_2 corresponds to the second Fourier component. The bilayer thickness is well defined, as judged from the intensity and the width of these peaks in the NG sample. On the other hand, much broader features are observed at corresponding length scales (Q_1 and Q_2) in the GR+ and GR− samples, as expected from a sample with a distribution in the thickness of the layers. The differences in the shape at the length scale corresponding to the average Q_2 values directly reveal the sign of the gradient. For example, for the GR− sample, the hump at higher Q in the Q_2 region is the widest. This effect arises because of an interference effect and is reversed when changing the sign of the gradient, as seen in Fig. 2 for the GR+ sample. The low-frequency humps arise from the presence of the Pd capping layer. The high-frequency fringes, the so-called Kiessig fringes,[28] represent the Fourier transform of the total thickness of the sample. The presence of these fringes at high Q is an indication of the well defined total thickness for the samples.

The reflectivity results were fitted using the GENX (Ref. 29) code. Interdiffusion and roughness reduce the intensity of the peaks at Q_1 and Q_2.[26] These values, together with the average thickness of the Fe magnetic layers and the V thickness, were determined by the fitting, cf. Table I. A represen-

TABLE I. Thicknesses of the Fe and V layers with the average roughnesses σ_r and interdiffusions σ_i as determined from the fitting. The Fe thickness refers to the weighted average of all the Fe layers in each sample. The uncertainties for each quantity are reported in the subscripts and superscripts.

Sample	Fe (Å)	V (Å)	σ_r (Å)	σ_i (Å)
NG	$4.49^{+0.01}_{-0.50}$	$10.51^{+0.03}_{-0.04}$	$2.3^{+1.48}_{-1.43}$	$2.4^{+0.01}_{-0.49}$
GR+	$3.67^{+0.01}_{-0.39}$	$11.47^{+0.02}_{-0.40}$	$1.3^{+1.1}_{-1.3}$	$2.4^{+0.84}_{-0.82}$
GR−	$3.50^{+0.2}_{-0.01}$	$11.52^{+0.07}_{-0.04}$	$1.7^{+0.40}_{-0.30}$	$2.9^{+0.69}_{-0.18}$

tative fitting of the results from the GR− sample is illustrated in Fig. 2 (red curve).

Information about the crystal structure and the out-of-plane coherence can be determined by x-ray analysis in the high Q region. Representative diffraction results are shown in Fig. 3. Q_0 corresponds to the main Bragg peak, representing the average distance between the atomic planes, including both the Fe and the V layers. The position of the Q_0 peaks of both the gradient samples is the same while the peak position of the NG sample is different. This is easily understood since the gradient samples have on average of 0.5 ML less Fe, resulting in slightly larger average lattice parameter.

The two side peaks of Q_0, namely, Q_{-1} and Q_{+1}, are the superlattice satellites. These peaks arise from the constructive interference between the periodic superlattice structures and the periodic lattice structure. The position of a peak with respect to Q_0 gives information about the bilayer thickness, and it can be compared with the positions Q_1 and Q_2 in the x-ray reflectivity results.

As shown in Fig. 3, the width of the Q_0 peak is not significantly affected by the presence of a thickness gradient because Fe and V have similar lattice parameters (2.87 and 3.03 Å) while the Q_{-1} satellite is significantly broadened. The broadening is absent in the Q_{+1} peak, which can be understood when considering the relation between the position of the peaks and the superlattice structure:

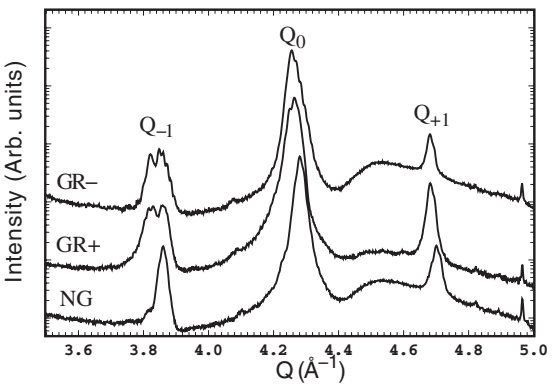

FIG. 3. X-ray diffraction spectra of the samples. The main peak Q_0 is related to the average lattice constant. The peaks Q_{-1} and Q_{+1} are the markers of the superlattice structure.

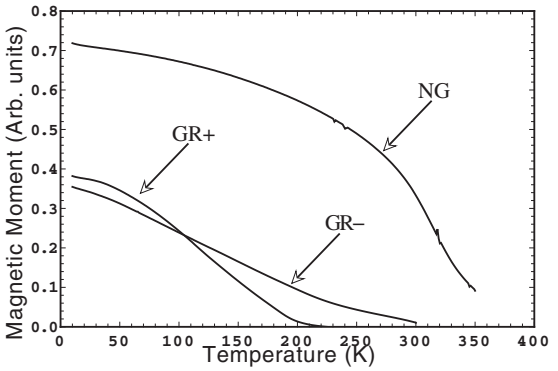

FIG. 4. Magnetization as a function of temperature for all the samples. The NG measurements are incomplete because of the limited temperature range of the SQUID.

$$Q_J = \frac{4\pi \sin \Theta}{\lambda} = 4\pi\left(\frac{n}{2\langle d_{hjk}\rangle} + \frac{n}{2\Lambda}\right). \tag{3}$$

Here, n is the order of the satellite, Λ is the average bilayer thickness, and $\langle d_{hjk}\rangle$ is the lattice parameter for the reflection with Miller indices (hjk). In the specific case of the gradient samples (GR+ and GR−), the variation in Λ is large. It is easy to show that $\delta Q/Q$ is larger when $Q < Q_0$ as compared to $Q > Q_0$, using Eq. (3) to provide a plausible explanation for the decrease in width with increasing Q.

The out-of-plane coherency was estimated using the full width at half maximum (FWHM), denoted in the following as $\Delta\omega$, of the Q_0 peak:[30]

$$\xi = 0.9\frac{2\pi}{Q_0 \Delta\omega}. \tag{4}$$

This approach typically yields a lower limit for the out-of-plane crystal coherence. An out-of-plane coherence length of ≈500 Å is found for the sample NG whereas the coherence length of the GR+ and GR− samples are somewhat smaller, ≈330 Å and ≈400 Å, respectively. Smaller coherence length is expected for the gradient samples due to the presence of a gradient in the layer thickness.

IV. MAGNETIC CHARACTERIZATION

A. SQUID measurements

The magnetic moment of the samples was determined using a SQUID. These measurements reveal the total magnetization of the samples. The temperature dependence of the magnetization was determined in an applied field of 6 mT. The results of these measurements are shown in Fig. 4. The measured magnetization is determined by two contributions: first, the contribution from the Fe atoms (μ_{Fe}) and second, the contribution from the interface region of V (μ_{V}). The magnetic contribution arising from the V interfaces reduces the obtained magnetization, as the interface regions of V are antiferromagnetically aligned to the Fe layers.[1,20,31–35] The resulting average magnetic moment per Fe atom ($\mu_{\mathrm{Fe}}^{\mathrm{eq}}$) for the NG sample at 10 K is $\mu_{\mathrm{Fe}}^{\mathrm{eq}} \approx 0.7\mu_B$, as compared to the bulk value $\mu_{\mathrm{Fe}} \approx 2.2\mu_B$. This is in agreement with other established results.[19,36,37]

The magnetic moment of the gradient samples is about one half of the NG sample. This is well in line with the expected results as the moment scales linearly with the thickness of the Fe layers in this thickness range.[6] The low-temperature magnetization of the gradient samples should be identical since the average Fe thickness of these should be the same.

As seen in Fig. 4, the magnetization is strongly affected by the presence and by the sign of the gradient. Furthermore, the gradient samples exhibit completely different asymptotic behavior as compared to what is observed for the NG sample. To obtain better understanding of these observations, we need to discuss the depth distribution of the changes in samples magnetization.

B. Spin-polarized neutron reflectivity

Neutrons are widely used to investigate magnetic structures[38] and dynamics in thin films,[39] as well as magnetic ordering in superlattices[26,40,41] and superstructures.[42] Here we use spin-polarized neutron reflectometry (PNR) for obtaining the magnetic profile within the samples. The PNR measurements, taken at the ADAM (Ref. 43) reflectometer at ILL (Grenoble, France), were performed at different temperatures for investigating the changes in the magnetic profile with temperature.

The magnetic ground state was determined at 12 K. A guide field of about 6 mT was applied during all of the measurements. A ^{3}He pencil detector was used and no spin-flip analysis was performed. The incident wavelength of the polarized neutron beam was $\lambda_0 = 4.4$ Å. The scattering plane is horizontal and the sample is mounted vertically. A magnetic field, generated by an electromagnet, is applied parallel to the plane of the samples.

In neutron reflectometry, the interaction of neutrons with matter is generally described by the Fermi pseudopotential $V^{\pm}$ (Ref. 44):

$$V^{\pm}(r) = \frac{2\pi\hbar^2}{m}(b_n \pm b_m)\delta(r), \tag{5}$$

where m denotes the mass of the neutron, b_n the nuclear scattering length, and b_m the magnetic scattering length. The nuclear scattering length b_n depends on the isotopes of the sample and the energy of the incoming neutrons. The average b_n for V is negative whereas the average b_n for Fe is positive.[45] The superscripts $V^{\pm}$ indicate that the scattering potential is different for neutrons aligned parallel (+) or antiparallel (−) to the internal field of the sample. The magnetic scattering length b_m is, consequently, proportional to the magnetization.

The calculation of the neutron reflectivity n_{N^0} is almost identical to the calculation of the Fresnel reflectivity for photons.[44] In a first approximation,

$$n_{N^0} = 1 - \frac{1}{2\pi}\rho\lambda^2(b_n \pm b_m), \tag{6}$$

where ρ is the number of nuclei per unit volume, and λ is the wavelength of the incident neutrons.

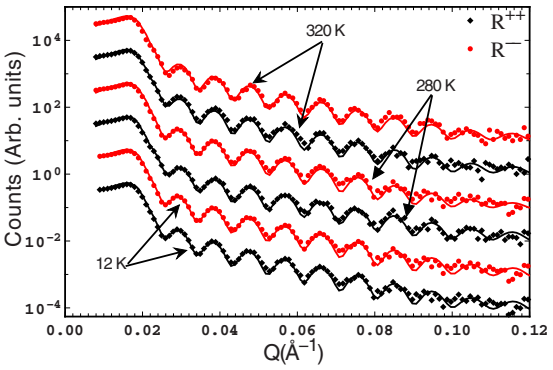

FIG. 5. (Color online) Neutron data and fits for the sample NG. The dots represent the raw data whereas the lines represent the fits.

1. *Reflectivity in the absence of thickness gradient*

The evolution of the magnetic profile for the NG sample was determined at four temperatures: 12, 280, 320, and 340 K. The measured intensity is labeled by $R^{\pm}$, where the superscript "+" represents measurements with neutron polarization along the applied field whereas the superscript "–" represents measurements with neutron polarization antiparallel to the applied field. The deduced spin asymmetry, S, is defined as

$$S = \frac{R^+ - R^-}{R^+ + R^-}. \tag{7}$$

At 340 K, the neutron reflectivity did not show any spin asymmetry. This is in contrast with the SQUID measurements which contain a ferromagnetic contribution at this temperature. In order to estimate the changes in the magnetic moment of the Fe layers, the reflectivity results were fitted by using the GENX code. The Kiessig fringes represent the relevant length scales, and the first fringe can be viewed as the first Fourier's component of the changes in the magnetization with depth. Thus, it carries predominantly information about the magnetization of the outermost layers in the sample. The higher order components can be viewed as additional terms describing the eventual gradient in the magnetization. We used three different models to fit the reflectivity results from the NG sample. In the first model (1), all the Fe layers are assumed to carry the same magnetic moment. In the second model (2), the topmost and bottom-most layers are assumed to have zero magnetization. In the third model (3), the two topmost and bottom-most layers are assumed to carry zero magnetization. The magnetization of the remainder of the Fe layers in models (2) and (3) is assumed to be the same, and is determined by the fitting process. These models are assumed to be representative for possible changes in magnetization and the quality of the fit (χ^2 analysis) is used as a qualifier for their validity. The structural parameters from the x-ray reflectivity data, see Table I, were used as fixed parameters in the fitting. The results are illustrated in Fig. 5, along with the experimental data for $T = 12$, 280, and 320 K.

At 12 K, the results are best described with a constant magnetization throughout the sample, leading to the conclu-

TABLE II. Fitted values for the Fe magnetic moments.

Temperature (K)	Magnetic moment (μ_B)
12	0.7 ± 0.5
280	0.5 ± 0.5
320	0.15 ± 0.2

sion that all the Fe layers carry the same magnetic moment. However, at elevated temperatures, a clear signature of a layer dependent magnetization becomes apparent. For example, at 280 K, the best fit is obtained using model (2) and at the highest temperature where spin splitting is still present (320 K), model (3) yields the best value of χ^2. This is related to the fact that the magnetization of the layers at the edges becomes smaller with respect to the inner ones while temperature increases, as discussed in Ref. 19. All magnetization parameters obtained from the fitting were consistent with the SQUID results, Table II.

2. Neutron reflectivity from gradient samples

Figure 6 shows the reflectivity results for all of the samples at 12 K. As seen in the figure, there is a big difference in the obtained spin asymmetry, which is largest for the NG sample. The second largest spin asymmetry is obtained in the GR− sample, consistent with the intended changes in the magnetization with depth, see Fig. 1. Finally, the GR+ sample exhibits almost negligible spin asymmetry at small Q values, as expected. Thus a qualitative agreement between the reflectivity results and the magnetic profile is established.

Two models were used for fitting the data. In the first model the Fe moment was assumed to change linearly with distance from the center of the sample, and in the second model the change in magnetization was assumed to be parabolic with the distance from the center of the sample. Both models were used to fit all the data, using the same initial values. In both cases, the best fit was found for a linear variation with thickness of the Fe magnetic moment. In Fig. 7 the raw data set and the fits for both GR+ and GR− are presented. These results are consistent with previous theoretical and experimental results.[34] The magnetizations determined by the neutron reflectivity were consistent with the SQUID results, that is, by summing up the fitted moments for Fe, we obtain an average moment consistent with the one determined by the SQUID measurements.

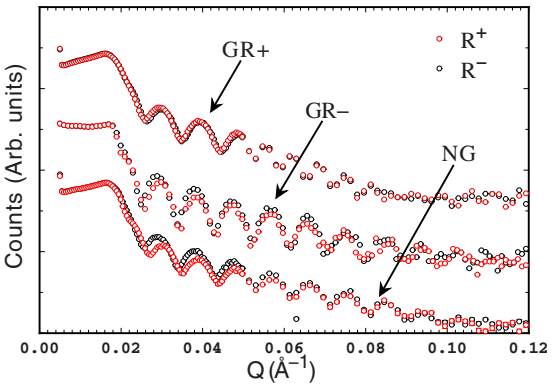

FIG. 6. (Color online) Reflectivity measurements at 12 K for the series of samples. The measurements are shifted in intensity for clarity.

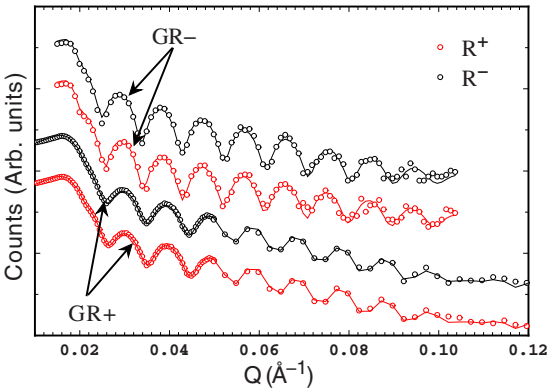

FIG. 7. (Color online) Reflectivity measurements at 12 K for the samples GR+ and GR−. The measurements are shifted in intensity for clarity.

C. MOKE measurements

1. Magnetization

The presence of a gradient in the magnetization called for a selective measurement of the magnetization in the near-surface region of the samples. Therefore, we performed MOKE measurements in an ac-MOKE setup, as described in Ref. 6. The 630 nm laser light used in the magneto-optical setup has an estimated penetration depth of ≈200 Å. Taking the unit cell to be [V(7)/Fe(3)], corresponding to ten monolayers of 1.5 Å, the MOKE response becomes weaker by a factor of $1/e$ in about nine to ten unit cells, taking into account the angle of the incident light. Thus, the signal from MOKE measurements will yield significantly larger contribution from the near-surface region as compared to the interior of the sample. The 50 Å Pd protective layer acts as an attenuator, reducing the magnetic response in the MOKE measurements.

The magnetization was measured along the Fe [100] axis (the easy axis for Fe). To facilitate the comparison of the results obtained from the different samples, we introduce the reduced temperature t, defined as $t=\frac{(T-T_c)}{T_c}$, where T_c is the ordering temperature. Representative hysteresis curves recorded at $\approx 0.45t$ (equivalent to 80 K for the GR+ case) are shown in Fig. 8. As apparent in the figure, a field of 6 mT is not sufficient to saturate the GR+ and GR− samples. There are thus slight differences in the field dependence of the magnetization of these samples but the overall properties appear to be similar at this reduced temperature.

The MOKE-hysteresis curves were continuously recorded while slowly increasing the temperature from 80 to 360 K. The $M(T)$ in the absence of field is deduced by the remanent magnetization of the hysteresis loops at all temperatures. In Fig. 9 the $M(T)$ curves for the samples are shown. The magnetization curve for the NG sample is close to what is ex-

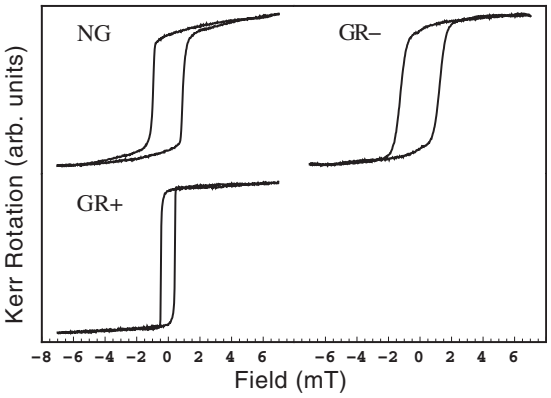

FIG. 8. Hysteresis loops for the three samples recorded at $\approx 0.45t$ (see text). The data sets are normalized.

pected for this class of materials, whereas both the GR+ and the GR− results are strongly deviating from what is expected from a uniform sample. To put this observation into a more quantitative perspective, we briefly outline the generally utilized description of the change in magnetization with temperature. Close to the ordering temperature the magnetization is classically described by the following equation:

$$M \sim (-t)^{\beta}, \quad H = 0, \quad t \to 0^{-}. \tag{8}$$

The exponent β takes on values depending on the spin (d) and the spatial (D) dimensionality of the system.[46,47] The $M(T)$ for the NG sample is easily fitted to Eq. (8) as was proposed by Elmers *et al.*[48] including a small distribution in $M(T)$. A single Fe layer with the same thickness as discussed here shows a two-dimensional (2D)-XY behavior[3] while in the actual NG superlattice, the interlayer exchange coupling is relatively strong and an exponent corresponding to a three-dimensional (3D) system would therefore be expected. In the presence of spin waves, which destroy the order,[49–51] the strength of the interlayer exchange coupling as a function of temperature T is given by:

$$J' = J'_0\left(1 - \frac{T}{T_c}\right)^{3/2}, \tag{9}$$

as theoretically found by Almeida *et al.*[52] and experimentally confirmed.[4,53] This effect is more pronounced when both the

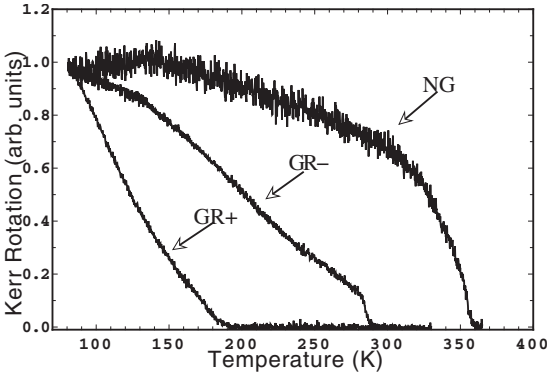

FIG. 9. MOKE results of the temperature dependence of the remanent magnetization. The Kerr rotation is normalized at 80 K for easing the comparison of the results.

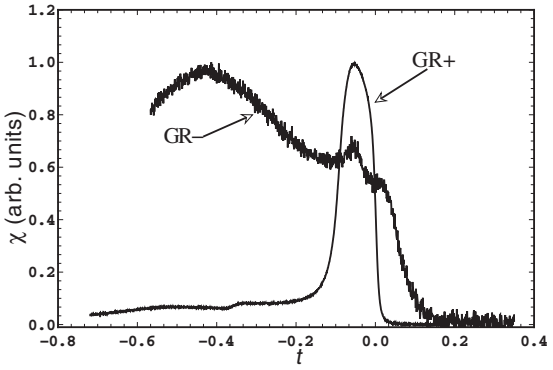

FIG. 10. Real part of the complex susceptibility as a function of t. For details, see text.

thickness of the spacer and the interlayer exchange coupling are small. This can be the reason why the resulting fitting yielded $\beta = 0.48$ which is much larger than the expected 3D critical exponent of $\beta \approx 0.34$ (Ref. 54) or the 2D $\beta \approx 0.23$.[46]

In this perspective it is meaningless to determine the exponents for the GR+ and GR− samples, as evident from the discussion above. However, we can still use the results for obtaining some insight in the apparent changes in the magnetization in the samples with temperature. First, if one attempts to fit the GR+ result with Eq. (8), the deduced exponent would be close to 1. Second, in order to fit the $M(T)$ for the GR sample, one cannot use a single power-law function. The second derivative of the magnetization changes sign when approaching the ordering temperature. In such cases, the change in J' as in Eq. (9) is a small effect as compared with the change in J in the framework of spin-wave dominated systems. Third, comparing Figs. 4 and 9 for the GR+ sample, the lower limit for the difference between the overall and the near-surface ordering temperature can be estimated. The MOKE results give an ordering temperature of about 190 K while SQUID yields an ordering temperature of ≈ 210 K. Thus the MOKE results are both qualitatively and quantitatively different from the magnetization results obtained by SQUID. But, the presence of an applied field in SQUID measurements, a field which alters the magnetic response, should be taken into account, for example, by stretching the tail above T_c (compare the magnetization of GR− sample in Fig. 4 with Fig. 9). These results are consistent with the presence of a critical region, which is wandering from the surface to the interior of the GR+ sample, implying a variation in T_c.

2. ac-MOKE magnetic susceptibility

The presence of a critical region can easily be determined by the same approach, using low ac field MOKE measurements. The ac susceptibility versus temperature, $\chi_{ac}(t)$, in a field of ≈ 0.2 mT and a frequency of 215 Hz is shown in Fig. 10 for both the gradient samples. As seen in the figure, the samples exhibit completely different behavior. While the GR+ sample exhibits a reasonable but wide maximum, the GR results cannot be described in terms of a single peak.

In the specific case of the GR sample, the ordering can be viewed as dominated by the presence of a magnetic link that

bridges two second-nearest neighbors (in this case the topmost half with the bottom-most half),[55] at the center of the sample, see Fig. 1(c). The central part of the sample has an inherent ordering temperature $T_{c,i}$ which is well below the $T_{c,i}$ of the outermost layers. Thus, in analogy with the melting process of a solid, the magnetization of the GR− sample can be viewed as "melting" from the inside. The layers that undergo a melting represent the critical region of the sample: the outermost magnetic layers which are probed in the susceptibility measurements are ferromagnetically coupled up to higher temperature with respect to the inner ones. This should give rise to broad response in the magnetic susceptibility, as observed here. Theoretical models have been developed in order to solve problems of weakly magnetically coupled trilayers with different critical temperature for each magnetic layer.[56,57] If the ordering temperature T_c of the magnetic layers were well spaced, then one should see two peaks in the magnetic susceptibility. In the present experiments, the T_c of the magnetic layers are close to each others. Thus, one can consider a continuum of peaks in the susceptibility measurements. Such continuum may be represented by wide temperature response as it happens in the case of the sample GR−.

By using similar argument, the magnetization of the near-surface region of the GR+ sample "melts" first, leaving the inner part of the sample in a ferromagnetic state. This critical region wanders into the sample, leaving the near-surface region in a paramagnetic state. As the susceptibility measurements probe the outermost layers, the transition in the center of the sample is not seen in the measurements of the GR+ sample. The considerations on the continuum peaks in the susceptibility measurements cannot be taken into account in such a case because the main contribution to the MOKE signal is coming by the weakly magnetic top layer.

V. CONCLUSIONS

The influence of a distribution of inherent ordering temperatures gives large and unexpected changes in the magnetization of coupled *XY*-layered magnets. When the outermost layers in the finite stack have the lowest inherent ordering temperature, the sample can be viewed as to melt from the outside in. This corresponds to regular surface melting with a wandering critical region. Unlike regular surface melting, the position of the critical region depends on the temperature. When the lowest inherent ordering temperature is in the center of the sample, the sample can be viewed to melt from the inside which yields significantly higher overall ordering temperature. The observed changes in the spontaneous magnetization with temperature is, in first approximation, close to linear. This difference cannot be reproduced by simplistic modeling of the magnetization.

The layer resolved magnetization of the superlattice with constant thickness of the magnetic layers revealed faster decrease in the magnetization of the outermost layers. This surface effect is a plausible reason for the abnormally high exponent observed in the MOKE measurements, in which the near-surface magnetization is predominantly probed. This calls for a strong precaution in the interpretation of the obtained exponents in magnetization measurements, indicating a possible origin of the large exponent observed in layered magnetic materials in the behavior of the near-surface magnetic properties different from the bulk one. This is clearly seen in the abnormally high $\beta \approx 0.48$, as compared to the expected ≈ 0.34. On the other hand, one must take also into account the change in J' both as function of temperature and as function of the distance from the magnetic layer. If this is taken into account, the resulting β becomes comprehensible.

These results give an insight in a possible origin of large exponents observed in layered magnetic materials. Furthermore the results highlight the need of exploring the influence on magnetic ordering of both the distribution in the inherent ordering temperature and the finite extension.

ACKNOWLEDGMENTS

The authors would like to acknowledge VR and KAW for financial support.

*bjorgvin.hjorvarsson@fysik.uu.se

[1] M. M. Schwickert, R. Coehoorn, M. A. Tomaz, E. Mayo, D. Lederman, W. L. O'Brien, T. Lin, and G. R. Harp, Phys. Rev. B **57**, 13681 (1998).
[2] A. Ney, F. Wilhelm, M. Farle, P. Poulopoulos, P. Srivastava, and K. Baberschke, Phys. Rev. B **59**, R3938 (1999).
[3] M. Pärnaste, M. Marcellini, and B. Hjörvarsson, J. Phys.: Condens. Matter **17**, L477 (2005).
[4] S. S. Kalarickal, X. Y. Xu, K. Lenz, W. Kuch, and K. Baberschke, Phys. Rev. B **75**, 224429 (2007).
[5] S. Andrieu, C. Chatelain, M. Lemine, B. Berche, and P. Bauer, Phys. Rev. Lett. **86**, 3883 (2001).
[6] M. Pärnaste, M. van Kampen, R. Brucas, and B. Hjörvarsson, Phys. Rev. B **71**, 104426 (2005).
[7] P. Bruno, *Interlayer Exchange Interactions in Magnetic Multilayers*, Magnetism: Molecules to Materials III (Wiley-VCH Verlag, Weinheim, Germany, 2002).
[8] M. D. Stiles, *Nanomagnetism: Ultrathin Films, Multilayers and Nanostructures*, Contemporary Concepts of Condensed Matter Science (Elsevier, New York, 2006), Vol. 1.
[9] B. Hjörvarsson, J. A. Dura, P. Isberg, T. Watanabe, T. J. Udovic, G. Andersson, and C. F. Majkrzak, Phys. Rev. Lett. **79**, 901 (1997).
[10] D. Labergerie, C. Sutter, H. Zabel, and B. Hjörvarsson, J. Magn. Magn. Mater. **192**, 238 (1999).
[11] U. Bovensiepen, F. Wilhelm, P. Srivastava, P. Poulopoulos, M. Farle, A. Ney, and K. Baberschke, Phys. Rev. Lett. **81**, 2368 (1998).
[12] P. Poulopoulos and K. Baberschke, J. Phys.: Condens. Matter **11**, 9495 (1999).
[13] A. Scherz, F. Wilhelm, U. Bovensiepen, P. Poulopoulos, H. Wende, and K. Baberschke, J. Magn. Magn. Mater. **236**, 1

(2001).
[14] F. Wilhelm, U. Bovensiepen, A. Scherz, P. Poulopoulos, A. Ney, H. Wende, G. Ceballos, and K. Baberschke, J. Magn. Magn. Mater. **222**, 163 (2000).
[15] K. Baberschke, Phys. Status Solidi B **245**, 174 (2008).
[16] G. A. T. Allan, Phys. Rev. B **1**, 352 (1970).
[17] F. J. Himpsel, J. E. Ortega, G. J. Mankey, and R. F. Willis, Adv. Phys. **47**, 511 (1998).
[18] Y. Li and K. Baberschke, Phys. Rev. Lett. **68**, 1208 (1992).
[19] M. Marcellini, M. Pärnaste, B. Hjörvarsson, G. Nowak, and H. Zabel, J. Magn. Magn. Mater. **321**, 1214 (2009).
[20] G. R. Harp, M. M. Schwickert, M. A. Tomaz, T. Lin, D. Lederman, E. Mayo, and W. L. O'Brien, IEEE Trans. Magn. **34**, 864 (1998).
[21] V. Meded, S. Olsson, P. Zahn, B. Hjövarsson, and S. Mirbt, Phys. Rev. B **69**, 205409 (2004).
[22] S. Olsson, A. M. Blixt, and B. Hjörvarsson, J. Phys.: Condens. Matter **17**, 2073 (2005).
[23] P. Granberg, P. Nordblad, P. Isberg, B. Hjörvarsson, and R. Wäppling, Phys. Rev. B **54**, 1199 (1996).
[24] P. Granberg, P. Isberg, E. B. Svedberg, B. Hjörvarsson, P. Nordblad, and R. Wäppling, J. Magn. Magn. Mater. **186**, 154 (1998).
[25] In the bulk, 1 ML of V is equivalent to 1.515 Å and 1 ML of Fe is equivalent to 1.435 Å.
[26] H. Zabel, Appl. Phys. A **58**, 159 (1994).
[27] P. F. Fewster, Rep. Prog. Phys. **59**, 1339 (1996).
[28] H. Kiessig, Ann. Phys. **402**, 715 (1931).
[29] M. Björck and G. Andersson, J. Appl. Crystallogr. **40**, 1174 (2007).
[30] B. E. Warren, *X-Ray Diffraction* (Dover, New York, 1990).
[31] A. Scherz, H. Wende, P. Poulopoulos, J. Lindner, K. Baberschke, P. Blomquist, R. Wappling, F. Wilhelm, and N. B. Brookes, Phys. Rev. B **64**, 180407(R) (2001).
[32] O. Eriksson, L. Bergqvist, E. Holmström, A. Bergman, O. LeBacq, S. Frota-Pessoa, B. Hjörvarsson, and L. Nordström, J. Phys.: Condens. Matter **15**, S599 (2003).
[33] M. A. Tomaz, W. J. Antel, W. L. O'Brien, and G. R. Harp, J. Phys.: Condens. Matter **9**, L179 (1997).
[34] M. Farle, A. N. Anisimov, K. Baberschke, J. Langer, and H. Maletta, Europhys. Lett. **49**, 658 (2000).
[35] M. Björck, M. Pärnaste, M. Marcellini, G. Andersson, and B. Hjörvarsson, J. Magn. Magn. Mater. **313**, 230 (2007).
[36] L.-C. Duda, P. Isberg, S. Mirbt, J.-H. Guo, B. Hjörvarsson, J. Nordgren, and P. Granberg, Phys. Rev. B **54**, 10393 (1996).
[37] K. Eftimova, A. M. Blixt, B. Hjörvarsson, and P. Svedlindh, J. Phys.: Condens. Matter **14**, 12575 (2002).
[38] H. Fritzsche, Y. T. Liu, J. Hauschild, and H. Maletta, Phys. Rev. B **70**, 214406 (2004).
[39] A. Schreyer, T. Schmitte, R. Siebrecht, P. Bodeker, H. Zabel, S. H. Lee, R. W. Erwin, C. F. Majkrzak, J. Kwo, and M. Hong, J. Appl. Phys. **87**, 5443 (2000).
[40] H. Zabel, Physica B **198**, 156 (1994).
[41] H. Zabel, R. Siebrecht, and A. Schreyer, Physica B **276-278**, 17 (2000).
[42] H. Zabel and K. Theis-Bröhl, J. Phys.: Condens. Matter **15**, S505 (2003).
[43] M. Wolff, K. Zhernenkov, and H. Zabel, Thin Solid Films **515**, 5712 (2007).
[44] G. L. Squires, *Introduction to the Theory of Thermal Neutron Scattering* (Dover, New York, 1996).
[45] For the tabulation of b_n see url http://www.ncnr.nist.gov/resources/n-lengths and for the computation of b_n see url http://www.ncnr.nist.gov/resources/sldcalc.html.
[46] S. T. Bramwell and P. C. W. Holdsworth, J. Phys.: Condens. Matter **5**, L53 (1993).
[47] J. J. Binney, N. J. Dowrick, A. J. Fisher, and M. E. J. Newman, *The Theory of Critical Phenomena* (Oxford University Press, Oxford, 1993).
[48] H.-J. Elmers, J. Hauschild, and U. Gradmann, Phys. Rev. B **54**, 15224 (1996).
[49] S. Schwieger and W. Nolting, Phys. Rev. B **69**, 224413 (2004).
[50] S. Schwieger, J. Kienert, and W. Nolting, Phys. Rev. B **71**, 174441 (2005).
[51] S. Schwieger, J. Kienert, K. Lenz, J. Lindner, K. Baberschke, and W. Nolting, Phys. Rev. Lett **98**, 057205 (2007).
[52] N. S. Almeida, D. L. Mills, and M. Teitelman, Phys. Rev. Lett. **75**, 733 (1995).
[53] J. Lindner, C. Rüdt, E. Kosubek, P. Poulopoulos, K. Baberschke, P. Blomquist, R. Wäppling, and D. L. Mills, Phys. Rev. Lett. **88**, 167206 (2002).
[54] K. Nho and E. Manousakis, Phys. Rev. B **59**, 11575 (1999).
[55] B. Hjörvarsson, Y. Kudasov, M. Wolff, T. Hase, C. Chacon, M. van Kampen, P. Nordblad, A. Liebig, and H. Zabel, Europhys. Lett. **81**, 17008 (2008).
[56] P. J. Jensen, K. H. Bennemann, K. Baberschke, P. Poulopoulos, and M. Farle, J. Appl. Phys. **87**, 6692 (2000).
[57] L. Bergqvist and O. Eriksson, J. Phys.: Condens. Matter **18**, 4853 (2006).